ACS APPLIED MATERIALS & INTERFACES

Research Article

www.acsami.org

Oxygen Vacancy Induced Band-Gap Narrowing and Enhanced Visible Light Photocatalytic Activity of ZnO

Junpeng Wang,[†] Zeyan Wang,[†] Baibiao Huang,*[,†] Yandong Ma,[‡] Yuanyuan Liu,[†] Xiaoyan Qin,[†] Xiaoyang Zhang,[†] and Ying Dai[‡]

[†]State Key Lab of Crystal Materials, Shandong University, Jinan 250100, China

[‡]School of Physics, Shandong University, Jinan 250100, China

Supporting Information

ABSTRACT: Oxygen vacancies in crystal have important impacts on the electronic properties of ZnO. With ZnO_2 as precursors, we introduce a high concentration of oxygen vacancies into ZnO successfully. The obtained ZnO exhibits a yellow color, and the absorption edge shifts to longer wavelength. Raman and XPS spectra reveal that the concentration of oxygen vacancies in the ZnO decreased when the samples are annealed at higher temperature in air. It is consistent with the theory calculation. The increasing of oxygen vacancies results in a narrowing bandgap and increases the visible light absorption of the ZnO. The narrowing bandgap can be confirmed by the enhancement of the photocurrent response when the ZnO was irradiated with visible light. The ZnO with oxygen vacancies are found to be efficient for photodecomposition of 2,4-dichlorophenol under visible light irradiation.

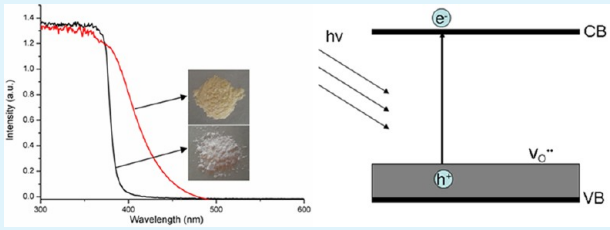

KEYWORDS: *zinc oxide, oxygen vacancy, zinc peroxide, band gap narrowing, photocatalysis*

INTRODUCTION

ZnO is an important wide band gap semiconductor material, which has been widely used in catalysis, ceramics, sensors, and optoelectronic devices, due to its excellent optical, peizoelectrical, and magnetic properties.[1−7] In recent years, the photocatalytic properties were also extensively studied.[8−12] Owing to the good photoelectric conversion properties and rapid photoresponse, ZnO exhibits high photocatalytic efficiencies on decomposing organic pollutants in water. Additionally, ZnO is nontoxic, abundant in reserves, and easy to obtain, which make it an ideal candidate for practical applications on environmental treatments.

However, the wide band gap of ZnO greatly limits the light responding range, which can only absorb ultraviolet light (λ < 380 nm) and seriously limits the photocatalytic efficiencies. It has become an important issue to expand the visible light response of ZnO for practical applications. In previous studies, many researchers have characterized the thermochromism properties of ZnO,[13−16] where ZnO turns from white to yellow when treated at high temperature, and the color change was attributed to the increase of oxygen vacancy related disorders at high temperatures. This work provides us a way to effectively expand the visible light absorption by introducing oxygen vacancies in ZnO materials. Compared with the conventional doping methods, oxygen vacancy is a kind of self-doping without introducing any impurity elements, which is more favorable on preserving the intrinsic crystal structures of ZnO and leads to enhanced photocatalytic performances under visible light irradiation. The oxygen vacancy induced visible light absorption and enhanced photocatalytic performances have been reported on TiO_2.[17,18] There is also a lot of research focused on the relationship between the oxygen defects and photocatalytic activity of ZnO;[10−12,19−21] however, oxygen vacancy induced band gap narrowing visible light photocatalytic performances in ZnO have never been systematically investigated yet.

On the synthesis of oxygen vacancy rich ZnO samples, there is still a great challenge. The oxygen vacancies in ZnO are unstable after high temperature annealing treatment, which would gradually transform from yellow to white again when it is cooled down to room temperature. Additionally, the concentrations of oxygen vacancies are usually low, which would not be adequate to expand the visible light absorption obviously. Uekawa et al. reported the synthesis of nonstoichiometric ZnO nanoparticles by decomposition of ZnO_2 precursors,[22,23] and recently, Jobic et al. also obtained stable P-type N-doped ZnO using ZnO_2 precursors.[24] Innovated by these works, it could be a simple strategy to introduce oxygen defects into ZnO crystal lattices by the decomposition of O_2^{2-}. Herein, we prepared ZnO by annealing ZnO_2 under different atmospheres and further confirmed the oxygen defects are oxygen vacancies. We investigated the effects of annealing temperatures on the concentration of oxygen vacancies in as-prepared ZnO systematically as well as their oxygen vacancy induced visible

Received: May 12, 2012
Accepted: July 11, 2012
Published: July 11, 2012

   dx.doi.org/10.1021/am300835p | ACS Appl. Mater. Interfaces 2012, 4, 4024−4030

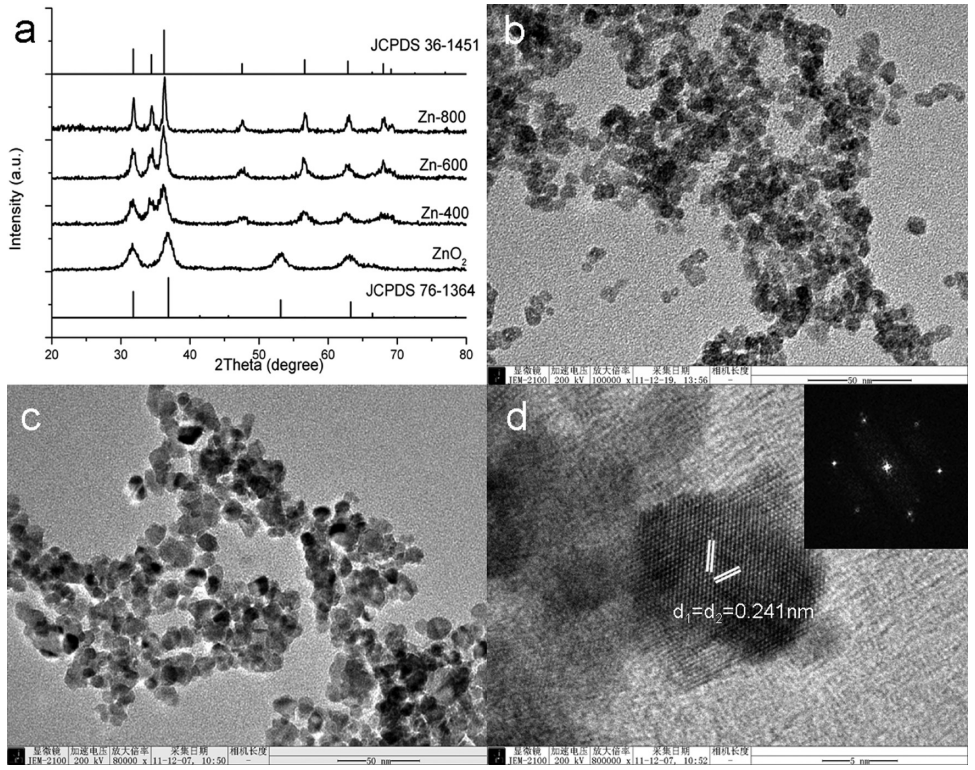

Figure 1. (a) Evolution of XRD patterns from ZnO_2 to ZnO under different annealing temperatures with Standard PDF card of ZnO and ZnO_2 was given as reference; (b) TEM images of the ZnO_2 precursor; (c) TEM images of the obtained V_O-400 samples and (d) corresponding high-resolution TEM image; the inset shows the short-time Fourier transform.

light photocatalytic properties. Our experimental results indicate the presence of oxygen vacancies in ZnO can effectively expand the visible light absorption range of ZnO and effectively enhance their visible light photocatalytic efficiencies. Higher oxygen vacancy concentrations would lead to stronger visible light absorption. Combined with theoretical calculations, a mechanism for the narrowing of ZnO band gaps and the enhancement on the photocatalytic performances is also proposed.

EXPERIMENTAL SECTION

Preparation of ZnO. The ZnO_2 nanoparticles were prepared according to the method proposed by Uekawa et al.[22] In detail, 100 mL of $Zn(NO_3)_2$ aqueous solution (0.2 M) and 100 mL of NaOH aqueous solution (0.2 M) were mixed and stirred for 2 h; the precipitate was separated by filtration. Then, the precipitate was separated to two parts, one was annealed in air at 400 °C for 2 h to obtain samples as ZnO reference, denoted as sample ZnO-ref, and the other was dispersed into 100 mL of H_2O_2 aqueous solution (1 M). The dispersed solution was kept at 75 °C for 2 h, and then, the precipitate was separated by centrifugation and dried at 75 °C; ZnO_2 powders were obtained. The as-obtained ZnO_2 powders were subsequently annealed in air for 2 h at 400 °C, 600 °C, and 800 °C, respectively; the obtained samples were denoted as V_O-400, V_O-600, and V_O-800 so as to distinguish from the ZnO-ref. To investigate the effect of annealing ambience on samples, ZnO_2 was also annealed under Ar flow (100 mL/min) at 800 °C for 2 h; the obtained samples were denoted as Ar-800 samples.

Characterization. X-ray diffraction (XRD) patterns were recorded on a powder diffractometer (Bruker AXS D8) with a Cu Kα X-ray tube. The crystal morphology was characterized by a high resolution transmission electron microscope (HRTEM) (JEOL-2100, 200 KV). Raman spectra were measured on Horiba LabRAM HR system with laser excitation of 532 nm. The chemical states of ZnO samples were characterized by X-ray photoelectron spectroscopy (XPS) in a Thermo Fisher Scientific Escalab 250 spectrometer with monochromatized Al Kα excitation, and C_{1s} (284.6 eV) was used to calibrate the peak positions of the elements. UV−vis diffuse reflectance spectra were recorded using a Shimadzu UV 2550 specteophotometer equipped with an interating sphere.

Calculation Details. Our predictions are based on the density functional theory (DFT) using generalized gradient approximation (GGA)[25] for exchange−correlation potential. We have used Perdew−Burke−Ernzerhof (PBE) functional for GGA as implemented in the Vienna ab initio Simulation Package (VASP).[26,27] The Brillouin zone is represented by the set of 9 × 9 × 7 k-points (for the 2*2*2) and 5 × 5 × 5 k-points (for the 3*3*2)[28,29] for the geometry optimizations and the static total energy calculations. The energy cutoffs, convergence in energy, and force are set to 400 eV, 10−4 eV, and 0.02 eV/Å, respectively. The positions of all the atoms in the supercell were fully relaxed.

Photocatalytic Activity Test. The photocatalytic activities of the ZnO samples were evaluated by the degradation of 2,4-dichlorophenol under visible light irradiation. A 300 W Xe lamp (PLS-SXE300, Beijing Trusttech Co. Ltd.) equipped with an ultraviolet cutoff filter was employed as the light source to provide visible light ($\lambda \geq 400$ nm). In a typical run, 50 mg of photocatalysts was dispersed in 100 mL of 2.4-dichlorophenol aqueous solution (20 mg L^{-1}) in a 200 mL Pyres glass. The solution was continuously stirred and kept in the dark for 1 h to establish adsorption−desorption equilibrium before being irradiated under visible light. The concentration of 2,4-dichlorophenol was monitored by a UV−vis spectrophotometer. Chemical oxygen demand (COD) concentration was also measured to monitor the decomposition of 2,4- dichlorophenol by permanganate titration.

Photo-Electrochemical Measurements. The photocurrent experiments were performed using a Princeton Applied Research (PAR) model 263A potentiostat/galvanostat. Ten mg of as-prepared ZnO sample and 15 mg of PEG-20000 were added in 4 mL of water, forming a uniform suspension after 10 min of ultrasonic treatment. The suspension was spin coated on a piece of FTO glass (1*1.5 cm^2) at a speed of 300 rps, then dried, and heated at 400 °C for 15 min. The

FTO glass was used as working electrode, and a 300 W Xe lamp (PLS-SXE300, Beijing Trusttech Co. Ltd.) was used as the light source (an ultraviolet cutoff filter was equipped to provide visible light ($\lambda \geq 400$ nm)). The FTO glass coating with our ZnO samples was used as a working electrode; a platinum sheet and an Ag/AgCl electrode were used as counter and reference electrodes, respectively. The electrolyte solution was a Na_2SO_4 aqueous solution (0.2 mol L^{-1}).

RESULTS AND DISCUSSION

The crystal structures of as-prepared ZnO_2 and the samples obtained after annealing under different temperatures were investigated by X-ray diffraction (XRD). As shown in Figure 1a, the peaks at 2θ = 31.8°, 36.9°, 53.1°, and 63.2° could be assigned to the (111), (200), (220), and (311) lattice planes of the cubic ZnO_2 (JCPDS 76-1364), and the wide peaks also indicate the small particles sizes of the ZnO_2 samples. The samples after annealing under different temperatures all exhibit a hexagonal wurtzite structure (JCPDS No. 36-1451) without any impurity phases, and the crystallinity of the sample was improved obviously with the increase of annealing temperatures. Figure 1b,c shows the TEM images of the ZnO_2 precursor and the ZnO samples annealed at 400 °C, both of which have a small crystal size; the diameter of the crystal is about 10 nm around. Figure 1d shows the high-resolution TEM images of the V_O-400 sample; the lattice spacing is about 0.241 nm, corresponding to the (101) planes of wurtzite ZnO. The distinguished two-dimensional lattice fringes and the short-time Fourier transform indicate that the obtained ZnO sample is well crystallized.

The Raman spectra of the ZnO samples annealed under different temperatures are shown in Figure 2. From the spectra,

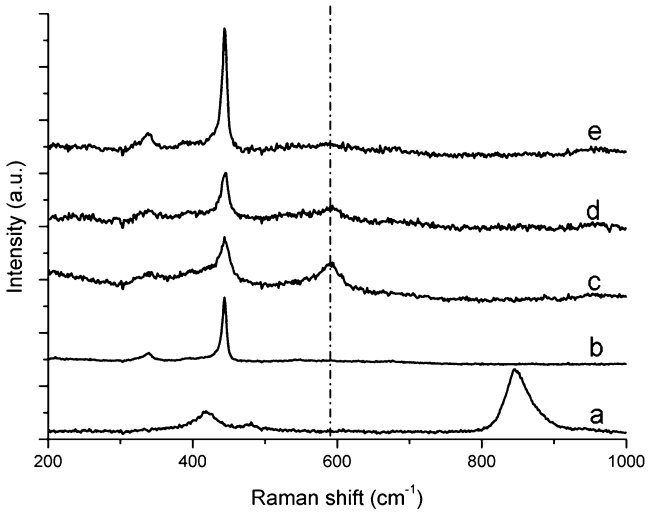

Figure 2. Room-temperature Raman spectra of (a) ZnO_2 and (b) ZnO reference and the ZnO obtained after annealing at different temperatures. (c) V_O-400, (d) V_O-600, and (e) V_O-800.

we can find that the characteristic peak of ZnO_2 samples located at 840 cm^{-1}, which can be assigned to the stretching band of the O−O bond of the peroxo ion (O_2^{2-}).[23,24] For ZnO samples, including the ZnO reference and the samples prepared from ZnO_2 precursors, a peak at 437 cm^{-1} corresponding to the typical vibration modes of wurtzite ZnO can be observed,[30,31] and the peak intensity for the samples prepared by the annealing of ZnO_2 precursors under different temperatures increased with the increase of annealing temperatures. Meanwhile, a new vibration mode around 590 cm^{-1} can also be observed for the ZnO samples prepared from ZnO_2 precursors, which was absent for the ZnO-ref prepared from $Zn(OH)_2$ precursors. This peak can be assigned to the contribution of O vacancies,[32,33] which resulted from the decomposition of ZnO_2 following the processes as shown in eqs 1−3. In the case of decomposition of the O_2^{2-} ions, eq 2 can easily occur because the presence of the O^{2-} ions around the decomposition atmosphere shifts the disproportionate reaction to the reduction side, and then, it is difficult for the oxidation reaction (eq 3) to occur.[23] Therefore, O vacancies can be easily formed during this process. The numbers of O vacancies can be easily controlled by changing the annealing temperatures. As shown in Figure 3c−e, the vibration peak corresponding to the O vacancies decreased with the increasing of annealing temperatures. As the annealing temperature is 800 °C, the vibration around 590 cm^{-1} almost disappeared. This can be attributed to the decrease of the O vacancies with the improvement of crystalline in the annealing process.

$$O_2^{2-} \rightarrow O_2 + 1/2O_2 \quad (1)$$

$$O_2^{2-} \rightarrow O_2 + 2e^- \quad (2)$$

$$O_2^{2-} + 2e^- \rightarrow 2O^{2-} \quad (3)$$

To gain more insight into the oxygen vacancies in the ZnO samples, the chemical states of O were investigated by XPS, and the XPS spectra for O_{1s} are shown in Figure 3. The O_{1s} spectra of the ZnO samples can be described as the superposition of three peaks by Gaussian distribution, located around 530.2 eV, 531.8 eV, and 533.4 eV, respectively. The O_{1s} peak at 533.4 eV is usually attributed to the presence of loosely bound oxygen on the surface of ZnO.[34] The low binding energy component located at 530.2 eV is attributed to the O^{2-} ions in wurtzite structure of a hexagonal Zn^{2+} ion array.[35] The medium binding energy component, centered at 531.8 eV, is associated with O^{2-} in the oxygen deficient regions with the matrix of ZnO.[35,36] It is believed that the intensity of this peak is connected to the variations in the concentration of oxygen vacancies. Therefore, changes in the intensity of this component may be connected in part to the variations in the concentration of oxygen vacancies, and in the O_{1s} spectra, we can find that the peak at 531.8 eV is obviously stronger in the ZnO sample obtained at 400 °C; the intensity of this peak decreased with increasing annealing temperature, as Table S1 (Supporting Information) shows, while the area ratio of the peak at 531.8 eV to the one at 530.2 eV is about 0.95, and this ratio is only 0.41 in the ZnO reference. It suggests that the oxygen vacancies in ZnO samples were reduced when treated with high temperature annealing; this is consistent with the former conclusion and the Raman result.

To evaluate the effect of oxygen vacancy on the energy gap of the ZnO samples prepared under different conditions, the optical properties of ZnO_2 and ZnO samples were probed by UV−visible diffuse reflectance spectroscopy. From Figure 4, we can find that ZnO_2 only responds to ultraviolet light, and the ZnO-ref prepared by annealing $Zn(OH)_2$ only responds to the light less than 380 nm; the calculated energy gap for ZnO_2 and ZnO-ref are about 3.8 and 3.2 eV, respectively, in accordance with the previous reports. All ZnO samples obtained by annealing ZnO_2 exhibit a red shift to longer wavelength compared with the ZnO reference. Compared with the white color of ZnO-ref, the sample annealed at 400 °C had a pale

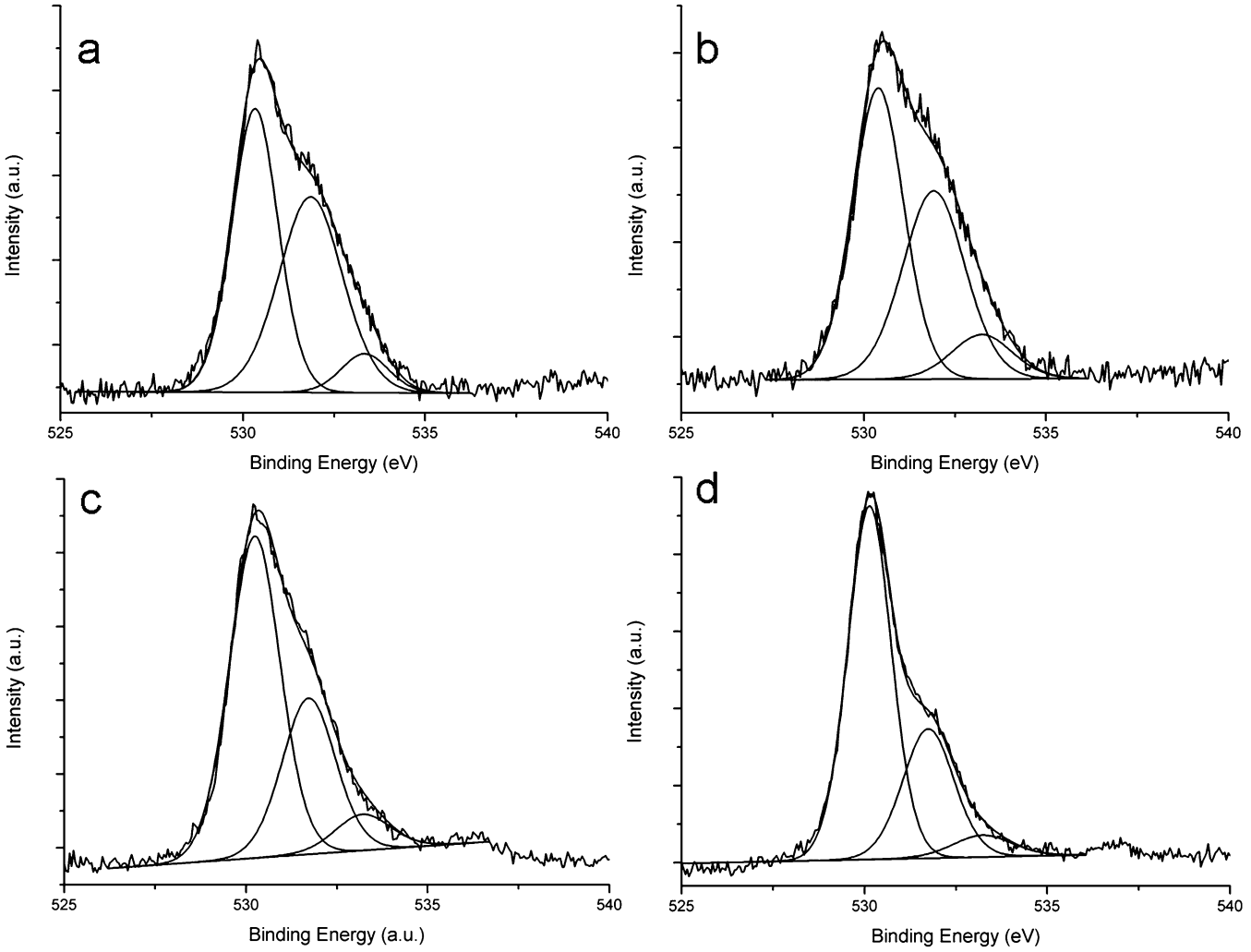

Figure 3. O 1s XPS spectroscopic spectra of the ZnO samples obtained by annealed ZnO_2 at different temperatures. (a) V_O-400, (b) V_O-600, (c) V_O-800, and (d) ZnO-ref.

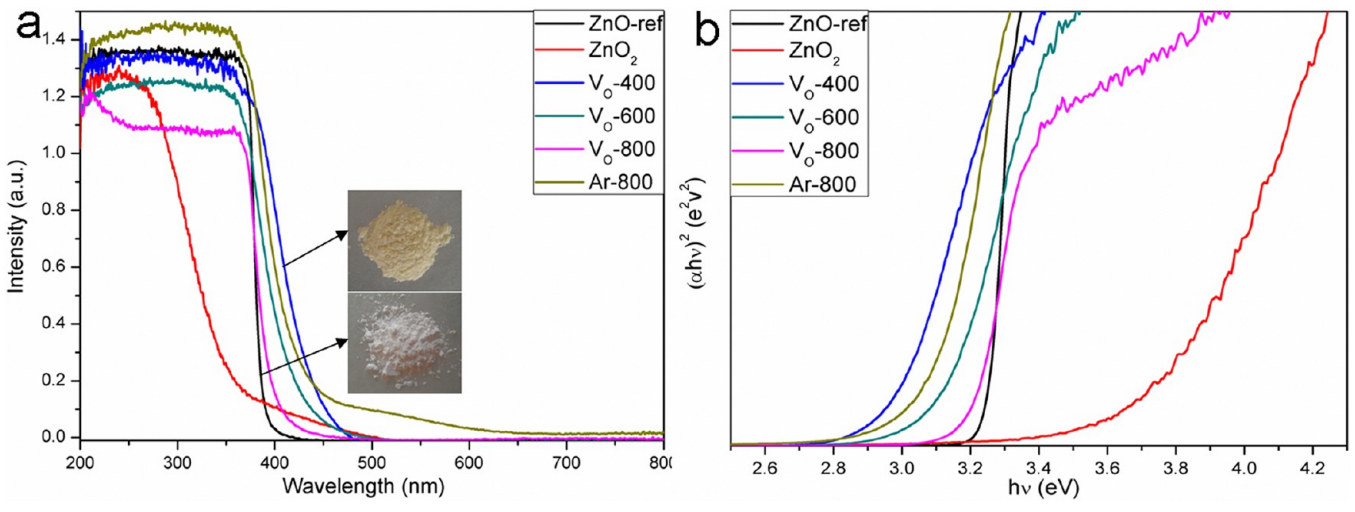

Figure 4. UV−visible diffuse reflectance spectra (a) and the energy band gap (b) of the as-prepared ZnO and ZnO2 samples.

yellow color and its absorption edge is around 500 nm. With the annealing temperature increasing, the absorption edge of the samples blue shifts to shorter wavelengths; the sample annealed at 800 °C exhibits a white color and almost has the same absorption edge with the ZnO-ref, except for a little tail around 420 nm. Combined with the Raman and XPS characterizations above, we can conclude that the O vacancies can effectively extend the visible light absorption of ZnO, and the band gap narrowing is closely related to the O vacancy

dx.doi.org/10.1021/am300835p | ACS Appl. Mater. Interfaces 2012, 4, 4024−4030

concentrations; i.e., ZnO-400 with the highest O vacancy concentrations has the best visible light response.

To further confirm this conclusion, we annealed the ZnO_2 precursor at 800 °C in an Ar atmosphere. In an oxygen-free condition, the oxygen vacancy should be preserved even after high temperature annealing; namely, compared with that annealed in the air condition, the obtained ZnO samples should have a narrower energy gap. As we anticipated, the obtained Ar-800 sample exhibits a pale yellow color as the ZnO samples obtained at 400 °C in air, and from the UV−visible diffuse reflectance spectra shown in Figure 4, the Ar-800 sample has no obvious blue shift than the sample annealed in lower temperature. Furthermore, the absorption edge of the Ar-800 sample even has a long tail extended at a wavelength of around 600 nm; this can be attributed to the O vacancies being preserved in an oxygen-free condition.

A series of first principles calculations has been performed to assess the influence of the presence of oxygen vacancies on the electronic properties of ZnO, and the corresponding electronic structures are presented in Figure 5. As Figure 5a illustrates, it is evident that the defect-free ZnO is a semiconductor with a band gap of about 1 eV. While introducing an oxygen vacancy in a 3*3*2 super cell, as shown in Figure 5b (the structure model of oxygen vacancy in a 3*3*2 super cell was shown in Figure 6), impurity state appears near the valence band edge,

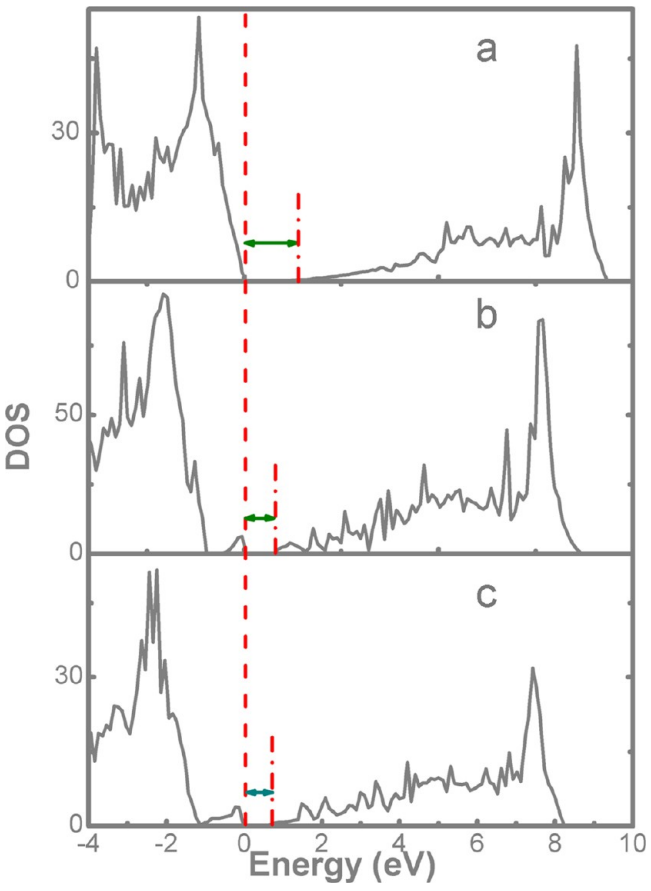

Figure 5. Calculated density of electronic states (DOS) for ZnO. The zero of the energy is taken at the top of the valence band of the defect-free ZnO crystal. (a) Defect-free, stoichiometric crystal (in a 2*2*2 super cell). (b) Model containing an oxygen vacancy per 36 oxygen atoms (in a 3*3*2 super cell). (c) Model containing an oxygen vacancy per 16 oxygen atoms (in a 2*2*2 super cell).

which is consistent with the previous results.[37] Besides, when the concentration of oxygen vacancies is increased, as shown in Figure 5c, the impurity states become more delocalized and overlap with the valence band edge, resulting to the band gap narrowing. Scheme 1 shows the influence of O vacancy concentrations on the band structures of as-prepared ZnO prepared from ZnO_2 precursors. However, the impurity level does not change the band gap when the oxygen vacancies concentration is low. While lots of oxygen vacancies exist in ZnO, the impurity states become more delocalized, overlap with the valence band edge, and raise the position of the valence band, making ZnO more efficient in absorption of the visible light. On the basis of these results, the redshift of the absorption edge presented in Figure 4 could be easily understood.

The photocatalytic activity of the as-prepared ZnO samples was evaluated by the photodegradation of 2,4-dichlorophenol under visible light (λ > 400 nm) irradiation (Figure 7). The ZnO reference shows low activity in 2,4-dichlorophenol photodegradation owing to its wide band gap, and only about 40% of 2,4-dichlorophenol was removed after 3 h of irradiation. In contrast, the samples prepared from ZnO_2 precursors show better activity in 2,4-dichlorophenol degradation. Among those, the sample annealed at 400 °C exhibits the highest activity and about 83% of 2,4-dichlorophenol was decomposed. COD values were also obtained to further confirm the degradation of 2,4-dichlorophenol. As Figure S1 (Supporting Information) shows, after 6 h of visible light irradation, the COD removal efficiencies were 53.1%, 45.4%, 36.4%, and 31.8% for different ZnO samples; the photocatalytic activity of the sample is V_O-400 > V_O-600 > V_O-800 >ZnO-ref. That is, the activities for the ZnO samples were gradually decreased with the increase of annealing temperatures. This can be attributed to the concentrations of oxygen vacancies, where it is high where the annealing temperature was low and decreases as the annealing temperature increased. The concentrations of O vacancies in the ZnO samples obtained at different annealing temperatures vary; this leads to different capacity of light absorption and photocatalytic activity.

To further confirm that the ZnO samples with more oxygen vacancies have stronger capacity in visible light absorption, the photocurrent response experiment was carried out. The photoelectrochemical measurements were conducted using a three-electrode cell; a Pt plate and Ag/AgCl electrode were used as the counter and reference electrodes. Figure 8 show the photocurrents measured for various ZnO samples as a function of time at zero bias voltage with light-on and light-off cycles. As expected, the sample annealed at 400 °C shows an obvious lager photocurrent under visible light (λ > 400 nm) irradiation, and all the samples prepared with ZnO_2 precursors have stronger photocurrent response than the samples prepared with $Zn(OH)_2$ precursor. The photocurrent decreases gradually with the samples' increasing annealing temperature; this can be attributed to the sample treated with a higher calcinations temperature being able to absorb less visible light. On the other hand, the enhancement of the photocurrents observed on the other samples further confirmed the decrease of their band gaps; the oxygen vacancies play a role of narrowing the band gap instead of just forming the active centers or trap centers.[11,38,39]

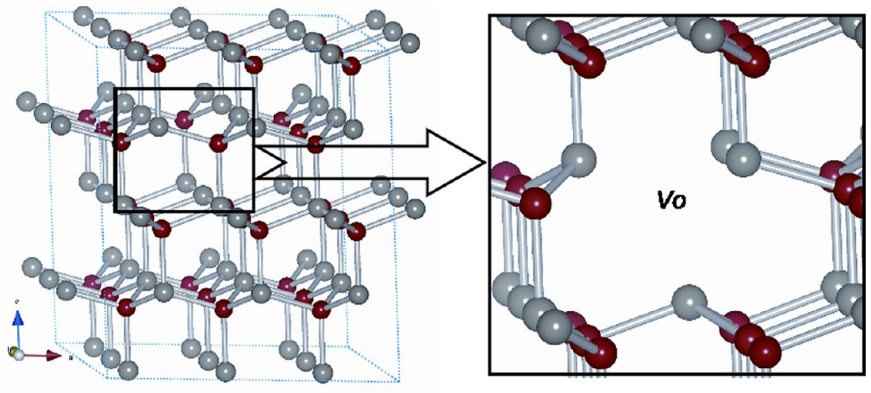

Figure 6. Structure model of oxygen vacancy in a 3*3*2 super cell; the balls in gray and red represent Zn and O atoms, respectively.

Scheme 1. Illustration of the Energy Bands for ZnO with Oxygen Vacancy Concentration and the Photoinduced Electronic Processes[a]

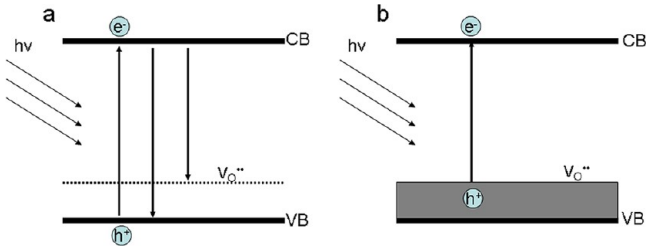

[a](a) Low oxygen concentration; (b) high oxygen concentration. CB, conduction band; VB, valence band; $V_O^{\cdot\cdot}$, oxygen vacancies.

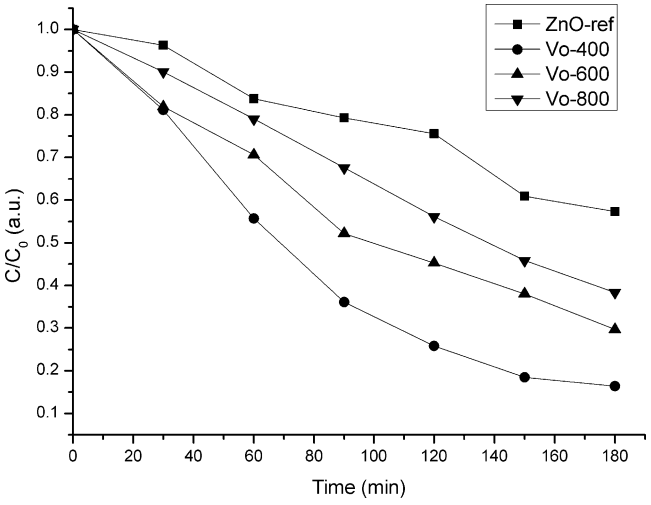

Figure 7. The photocatalytic degradation of 2,4-dichlorophenol over various photocatalysts under visible light irradiation.

CONCLUSION

To summarize, we obtained a yellowish ZnO with a narrowing band gap by decomposition of ZnO_2 precursors, and compared with the ZnO obtained with $Zn(OH)_2$ precursors, the oxygen vacancies are easily introduced into ZnO crystal for the instability of peroxide. From the Raman and XPS results, we can conclude that the high concentration of oxygen vacancies in the ZnO samples lead to the enhancement of visible light absorption capability. Not only is the role of oxygen as a trap center, but also the high concentration of oxygen vacancy creates an impurity level near the valence band and induces the band gap narrowing. The photocurrent experiments under visible light irradiation further confirm the enhanced visible light absorption capability of the ZnO samples synthesized with ZnO_2 precursors, and the ZnO samples obtained by annealing ZnO_2 precursors under different temperatures all exhibit better photocatalytic activity in photo decomposition of 2,4-dichlorophenol.

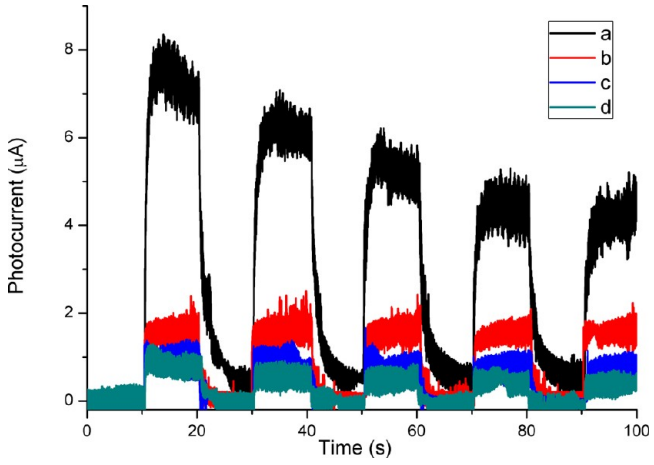

Figure 8. Photocurrent of ZnO annealed at (a) 400 °C, (b) 600 °C, (c) 800 °C, and (d) ZnO reference. The photoelectrodes were measured at zero bias voltage versus Ag/AgCl in 0.2 M Na_2SO_4 aqueous solution.

ASSOCIATED CONTENT

Supporting Information

Titration details; table of XPS peak information; figure of COD values after visible light irradiation with different ZnO samples. This material is available free of charge via the Internet at http://pubs.acs.org.

AUTHOR INFORMATION

Corresponding Author

*E-mail: bbhuang@sdu.edu.cn.

Notes

The authors declare no competing financial interest.

■ ACKNOWLEDGMENTS

This work is financially supported by the National Science Foundation of China (Nos. 51002091, 20973102, and 51021062), Specialized Research Fund for the Doctoral Program of Higher Education (20100131120028), the National Basic Research Program of China (No. 2007CB613302), and Natural Science Foundation of Shandong province (ZR2010BQ005).

■ REFERENCES

(1) Zeng, H. B.; Cai, W. P.; Liu, P. S.; Xu, X. X.; Zhou, H. J.; Klingshirn, C.; Kalt, H. *Acs Nano* **2008**, *2*, 1661.
(2) Zhang, H.; Wu, J. B.; Zhai, C. X.; Du, N.; Ma, X. Y.; Yang, D. *Nanotechnology* **2007**, *18*, 455604.
(3) Hu, X.; Gong, J.; Zhang, L.; Yu, J. C. *Adv. Mater.* **2008**, *20*, 4845.
(4) Shen, G. Z.; Bando, Y.; Liu, B.; Golberg, D.; Lee, C. *Adv. Funct. Mater.* **2006**, *16*, 410.
(5) Wang, Z. Y.; Huang, B. B.; Qin, X. Y.; Zhang, X. Y.; Wang, P.; Wei, J. Y.; Zhan, J.; Jing, X. Y.; Liu, H. X.; Xu, Z. H.; Cheng, H. F.; Wang, X. N.; Zheng, Z. K. *Mater. Lett.* **2009**, *63*, 130−132.
(6) Ueda, K.; Tabata, H.; Kawai, T. *Appl. Phys. Lett.* **2001**, *79*, 988.
(7) Wang, Z. L.; Song, J. H. *Science* **2006**, *312*, 242.
(8) Wang, Z. Y.; Huang, B. B.; Dai, Y.; Qin, X. Y.; Zhang, X. Y.; Wang, P.; Liu, H. X.; Yu, J. X. *J. Phys. Chem. C* **2009**, *113*, 4613.
(9) Sakthivel, S.; Neppolian, B.; Shankar, M. V.; Arabindoo, B.; Palanichamy, M.; Murugesan, V. *Sol. Energy Mater. Sol. Cells* **2003**, *77*, 65−82.
(10) Wang, J. C.; Liu, P.; Fu, X. Z.; Li, Z. H.; Han, W.; Wang, X. X. *Langmuir* **2009**, *25*, 1218−1223.
(11) Guo, M. Y.; Ng, A. M. C.; Liu, F. Z.; Djurisic, A. B.; Chan, W. K.; Su, H. M.; Wong, K. S. *J. Phys. Chem. C* **2011**, *115*, 11095−11101.
(12) Li, G. R.; Hu, T.; Pan, G. L.; Yan, T. Y.; Gao, X. P.; Zhu, H. Y. *J. Phys. Chem. C* **2008**, *112*, 11859−11864.
(13) Wiberg, E.; Holleman, A. F. *Inorganic Chemistry*; Academic Press: San Diego, CA, 2001.
(14) Aghamalyan, N. R.; Gambaryan, I. A.; Goulanian, E. Kh.; Hovsepyan, R. K.; Kostanyan, R. B.; Petrosyan, S. I.; Vardanyan, E. S.; Zerrouk, A. F. *Semicond. Sci. Technol.* **2003**, *18*, 525−529.
(15) Ye, J. D.; Gu, S. L.; Zhu, S. M.; Qin, F. S.; Liu, M.; Liu, W.; Zhou, X.; Hu, L. Q.; Zhang, R.; Shi, Y.; Zheng, Y. D. *J. Appl. Phys.* **2004**, *96*, 5308.
(16) Huo, Y.; Hu, Y. H. *Ind. Eng. Chem. Res.* **2012**, *51*, 1083−1085.
(17) Justicia, I.; Ordejon, P.; Canto, G.; Mozos, J. L.; Fraxedes, J.; Battiston, G. A.; Gerbasi, R.; Figueras, A. *Adv. Mater.* **2002**, *14*, 1399.
(18) Zuo, F.; Wang, L.; Wu, T.; Zhang, Z. Y.; Borchardt, D.; Feng, P. Y. *J. Am. Chem. Soc.* **2010**, *132*, 11856−11857.
(19) Zheng, Y.; Chen, C.; Zhan, Y.; Lin, X.; Zheng, Q.; Wei, K.; Zhu, J.; Zhu, Y. *Inorg. Chem.* **2007**, *46*, 6675−6682.
(20) Wang, H. H.; Xie, C. S. *Phys. E: Low-Dimens. Syst. Nanostruct.* **2008**, *40*, 2724−2729.
(21) Patil, A. B.; Patil, K. R.; Pardeshi, S. K. *J. Solid State Chem.* **2011**, *184*, 3273−3279.
(22) Uekawa, N.; Kajiwara, J.; Mochizuki, N.; Kakegawa, K.; Sasaki, Y. *Chem. Lett.* **2001**, *30*, 606.
(23) Uekawa, N.; Mochizuki, M.; Kajiwara, J.; Mori, F.; Wu, Y. J.; Kakegawa, K. *Phys. Chem. Chem. Phys.* **2003**, *5*, 929−934.
(24) Chavillon, B.; Cario, L.; Renaud, A.; Tessier, F.; Chevire, F.; Boujtita, M.; Pellegrin, Y.; Blart, E.; Smeigh, A.; Hammarstrom, L.; Odobel, F.; Jobic, S. *J. Am. Chem. Soc.* **2012**, *134*, 464−470.
(25) Perdew, J. P.; Burke, K.; Ernzerhof, M. *Phys. Rev. Lett.* **1996**, *77*, 3865.
(26) Kresse, G.; Furthmuller, J. *Phys. Rev. B: Condens. Matter* **1996**, *54*, 11169.
(27) Kresse, G.; Joubert, J. *Phys. Rev. B* **1999**, *59*, 1758.
(28) Monkhorst, H. J.; Pack, J. D. *Phys. Rev. B: Solid State* **1976**, *13*, 5188.
(29) Ma, Y. D.; Dai, Y.; Guo, M; Niu, C. W.; Zhu, Y. T.; Huang, B. B. *ACS Nano* **2012**, *6*, 1695−1701.
(30) Xing, Y. J.; Xi, Z. H.; Xue, Z. Q.; Zhang, X. D.; Song, J. H.; Wang, R. M.; Xu, J.; Song, Y.; Zhang, S. L.; Yu, D. P. *Appl. Phys. Lett.* **2003**, *83*, 1689.
(31) Li, C.; Hong, G.; Wang, P.; Yu, D.; Qi, L. *Chem. Mater.* **2009**, *21*, 891−897.
(32) Exarhos, G. J.; Sharma, S. K. *Thin Solid Films* **1995**, *270*, 27.
(33) Rajalakshmi, M.; Arora, A. K.; Bendre, B. S.; Mahamuni, S. *J. Appl. Phys.* **2000**, *87*, 2445.
(34) Fan, J. C. C.; Goodenough, J. B. *J. Appl. Phys.* **1977**, *40*, 3524.
(35) Park, S.; Ikegami, T.; Ebihara, K. *Thin Solid Films* **2006**, *513*, 90.
(36) Chen, M.; Wang, X.; Yu, Y. H.; Pei, Z. L.; Bai, X. D.; Sun, C.; Huang, R. F.; Wen, L. S. *Appl. Surf. Sci.* **2000**, *158*, 134.
(37) Janotti, A.; Van de Walle, C. G. *Appl. Phys. Lett.* **2005**, *87*, 122102.
(38) Salvador, P.; Garcia Gonzalez, M. L.; Munoz, F. *J. Phys. Chem.* **1992**, *96*, 10349.
(39) Liu, Y. Y.; Son, W.-J.; Lu, J. B.; Huang, B. B.; Dai, Y.; Whangbo, M.-H. *Chem.—Eur. J.* **2011**, *17*, 9342.